

DETC2001/DAC-21089

DESIGN OF COMPLIANT FORCE AND DISPLACEMENT AMPLIFICATION MICRO-MECHANISMS

Matthew B. Parkinson

Biomedical Engineering Department

Brian D. Jensen

Katsuo Kurabayashi

Department of Mechanical Engineering
University of Michigan
Ann Arbor, MI

ABSTRACT

In many MEMS applications, it is desirable to amplify the force or displacement of an actuator or transducer. Devices that amplify force or mechanical advantage typically achieve this at the expense of displacement or geometric advantage. Likewise, devices that amplify geometric advantage do so at the expense of mechanical advantage. This paper proposes a device topology based on a four-link mechanism with compliant segments in place of hinges. Finite-element analysis and optimization were used to develop a Pareto set of solutions quantifying the force / displacement trade-off for a variety of loading conditions. Depending on these conditions, this device is capable of multiplying force inputs by as much as 23.7 and displacement inputs by as much as 588. Efficiency of these designs improves as the two objectives (mechanical and geometric advantage) are considered jointly in a multicriteria optimization problem rather than individually.

INTRODUCTION

In many micro-mechanical applications, it is desirable to amplify the force or displacement of an actuator or a transducer. For example, levers have been used to improve the resolution of a resonant accelerometer by amplifying the force output [1], as well as amplifying stress in a micro tensile-test system [2]. Displacement amplification schemes have been used to make practical thermal actuators despite the inherently small strains induced by thermal heating, for example, in [3-6]. Displacement amplification has also been used to create usable micro-actuators using the small output displacement of piezo-electric

materials [7-10], as well as amplifying displacement output of electrostatic actuators to allow miniaturization of the actuator [11,12].

All of these force or displacement amplifying mechanisms are fully compliant; that is, their motion derives from the deformation of their parts rather than from rigid-body joints. The use of compliance has great advantages for MEMS because it allows mechanisms to operate without friction, wear or backlash, and because it allows complete systems to be created using fewer mask layers, potentially decreasing fabrication costs [13].

Previously, research in compliant mechanisms has addressed the design of compliant displacement amplifiers using size optimization of a known topology [14] and with the goal of distributing "compliance" throughout the entire mechanism. Canfield and Frecker [15] presented methods to generate optimal topologies within a given design space. These papers outline the need for such devices, as well as presenting results for sample design problems. This paper investigates a given mechanism topology to determine its ability to act as either a displacement or a force amplifier for a MEMS application. Specifically, size optimization of a prescribed topology is performed to find the Pareto set of designs using a multi-criteria approach, where the objective is to maximize mechanical and geometric advantage. When considering two objective functions, the Pareto set is the set of designs for which improvement of one objective can only be made at the expense of the other. Here, mechanical advantage is defined as the ratio of output force to input force, and geometric advantage is the ratio of output displacement to input displacement. Obviously,

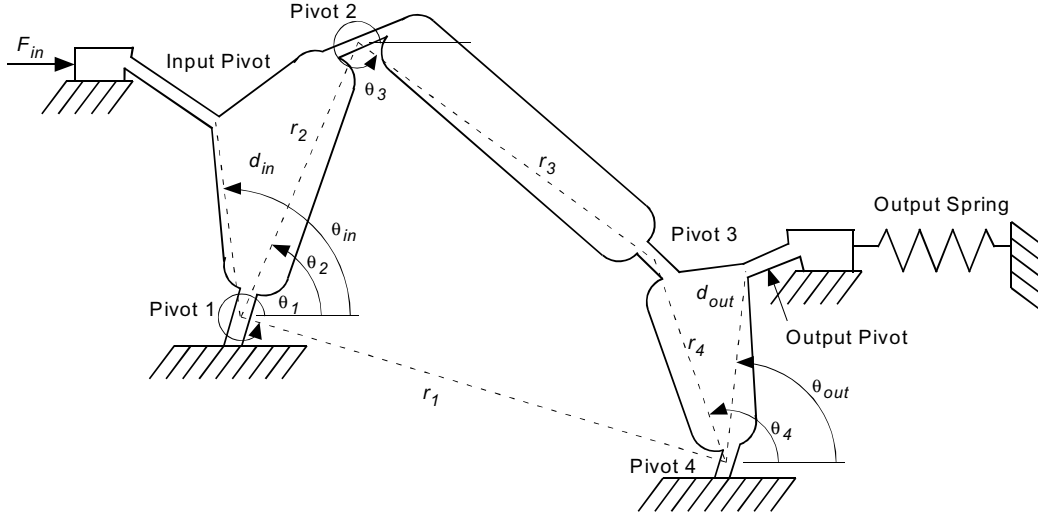


Figure 1. Parameterized model of the fully-compliant force or displacement amplifying mechanism.

these are competing objectives, allowing determination of a well-defined Pareto set for the compliant micro-mechanism, similar to the Pareto set produced by Cappelleri et al. [10] for a piezoceramic bimorph actuator. The Pareto set is compared for a wide range of output stiffness. The results show that the performance and efficiency of the optimal designs depends heavily on output load. They also demonstrate that the multi-criteria approach produces designs with better efficiency than a single-criteria approach. Finally, the chosen topology is demonstrated to perform well for designs optimized over a wide range of output loads.

PROBLEM DEFINITION

The topology investigated here is illustrated in Figure 1. It is generated by starting with a four-link mechanism. Rigid-body four-link mechanisms can create theoretically infinite mechanical or geometric advantages over small displacements, making this a reasonable starting topology. To create a fully compliant topology, each pin joint in the four-link topology is replaced with a flexural pivot whose center lies on the joint [16], and the input and output are linked to the input and output arms of the mechanism by additional flexural pivots. The input and output are chosen to act in a straight line horizontally, allowing the mechanism to be connected to an actuator or transducer operating in a straight line. In addition, the out-of-plane thickness is constant for the whole mechanism, allowing it to be micro-machined using planar lithography. The resulting topology is described by 32 parameters, which are:

r_1, r_2 , and r_4 - Equivalent link lengths for the mechanism, as illustrated in the figure

θ_{10}, θ_{20} , and θ_{40} - Initial angle of the equivalent links, as illustrated in the figure

d_{in} and d_{out} - length of the moment arm to the input and output pivots, as illustrated in the figure

θ_{din} and θ_{dout} - angle with respect to the horizontal of the input and output moment arms.

$l_1, l_2, l_3, l_4, l_{in}$, and l_{out} - length of pivots 1 through 4, as well as the input and output pivots

$t_1, t_2, t_3, t_4, t_{in}$, and t_{out} - thickness of pivots 1 through 4, as well as the input and output pivots

$\theta_{p1}, \theta_{p2}, \theta_{p3}, \theta_{p4}, \theta_{pin}$, and θ_{pout} - angles with respect to horizontal of each of the six pivots

h_z - out-of-plane thickness of the entire mechanism

t_{rigid} - the thickness of the relatively rigid members (assumed constant)

F_{in} - value of the input force

k_{out} - stiffness of the output spring

Note that the values of r_3 and θ_3 shown in Figure 1 are not used as parameters because they are dependent on the values of $r_1, r_2, r_4, \theta_{10}, \theta_{20}$, and θ_{40} . The in-plane thickness of the rigid members is given a constant value of t_{rigid} despite any real thickness changes in the mechanism (such as in the input and output members of the model shown in Figure 1). This is because as long as the rigid parts are significantly thicker than the flexible segments (more than about three times thicker), the compliance of the rigid segments is negligible compared to the compliance of the flexural pivots. This represents a “lumped compliance” rather than a “distributed compliance” approach—the stress constraints posed in the optimization problem will prevent failure. The stiffness of the output load is modeled using a spring of stiffness k_{out} . By varying this stiffness, the optimal design of this mechanism can be found over a wide range of output loads.

The FEM Model

The finite element model was created using nonlinear beam elements. These elements allow a combination of computational accuracy, including nonlinear deflection analysis, with easy

parameterization and meshing. The general mechanism topology was parameterized using the 32 variables outlined in the preceding section. These variables served as the input to the finite element model, which was solved in batch mode to allow an optimization program to control the selection of variable values. The displacements and reactions of the model were calculated for four values of input force, equal to $-F_{in}$, $-F_{in}/2$, $F_{in}/2$, and F_{in} . These four solutions allow determination of the linearity of the output over the range of input from $-F_{in}$ to F_{in} . The outputs of the finite element model were maximum stress in the mechanism, input displacement, output displacement, and output force for each level of input force. The material used for the finite element analysis was polysilicon, with assumed Young's modulus of 165 GPa and Poisson's ratio of 0.23. These values are representative of literature values, although substantial variation has been observed depending on deposition and etching parameters [17].

The Optimization Model

The finite element model was linked to a general nonlinear design optimization program using a c-code wrapper. Of the model parameters listed previously, four were chosen as parameters (listed in Table 1), and the remaining 28 as design variables. The parameters listed in the table were chosen to represent real expected values. For example, 10 μN of force is a common output force available from many electrostatic comb actuators, and 2 μm was chosen for h_z as a fairly normal value of out-of-plane thickness of many surface micro-machined structural layers. For the first optimization analyses, k_{out} was chosen to be 10 N/m. This is an intermediate stiffness, lying logarithmically between a fairly stiff output of 1000 N/m (such as might be expected from a resonant accelerometer) and a very weak output of 0.01 N/m. After generating a Pareto curve for $k_{out} = 10$ N/m, Pareto curves for several output stiffnesses across the listed range were produced.

The optimization problem for maximizing mechanical advantage is then

$$\begin{array}{ll} \text{maximize} & MA \\ \text{x} & \end{array} \quad (1)$$

$$\begin{array}{ll} \text{subject to} & \sigma_{max} \leq S_y \end{array} \quad (2)$$

Table 1: Parameter values for the optimization problem

Symbol	Description	Units	Value
l_{rigid}	width of rigid segments	μm	20
F_{in}	input force	μN	10
h_z	out-of-plane thickness	μm	2
k_{out}	output stiffness	N / m	0.01-1000

$$\% \text{ Nonlinearity} \leq 5\% \quad (3)$$

$$l_1 + r_2 + \frac{l_2}{2} \leq l_c \quad (4)$$

$$\frac{l_2}{2} + r_3 + \frac{l_3}{2} \leq l_c \quad (5)$$

$$l_4 + r_4 + \frac{l_3}{2} \leq l_c \quad (6)$$

$$l_1 + d_{in} + l_{in} \leq l_c \quad (7)$$

$$l_4 + d_{out} + l_{out} \leq l_c \quad (8)$$

where s_{max} is the maximum stress in the mechanism, S_y is the strength of the material (assumed to be 1 GPa for polysilicon), $\% \text{ Nonlinearity}$ is the maximum deviation (in percent) from linearity, and l_c is a rule-of-thumb maximum length. The nonlinearity is the maximum difference from the least-squares line through each of the four output points as well as zero. The rule-of-thumb maximum length is chosen to be 400 μm , a reasonable length of MEMS parts to avoid excessive stiction. Single-criteria optimization of the geometric advantage is identical to the problem statement above, with maximization of mechanical advantage replaced with maximization of geometric advantage.

Given the large number of design variables, length of time required for each FEA solution (about 10-20 seconds), and the nonlinearity of the design space, a combination of optimization algorithms was used. First, the stochastic Simulated Annealing (SA) algorithm was used to quickly and randomly search the entire design space to find the most promising region. This was used as a starting point for the gradient-driven GRG method, which refined the design until optimal performance was achieved. A treatment of the specific SA algorithm used is found in [18]. Information on the GRG algorithm used is found in [19].

RESULTS

Mechanical Advantage

The mechanical advantage optimization problem, Eq. (1), was solved using the method outlined above. The resulting design, which maximizes the force amplification for the chosen topology under the loading condition $k_{out} = 10$ N/m, is shown in Figure 2. The active constraints for this design are Eq. (3), the nonlinearity constraint, and Eq. (7), which limits the total length of the input arm. The input force will be amplified by a factor of 6.25 for this design.

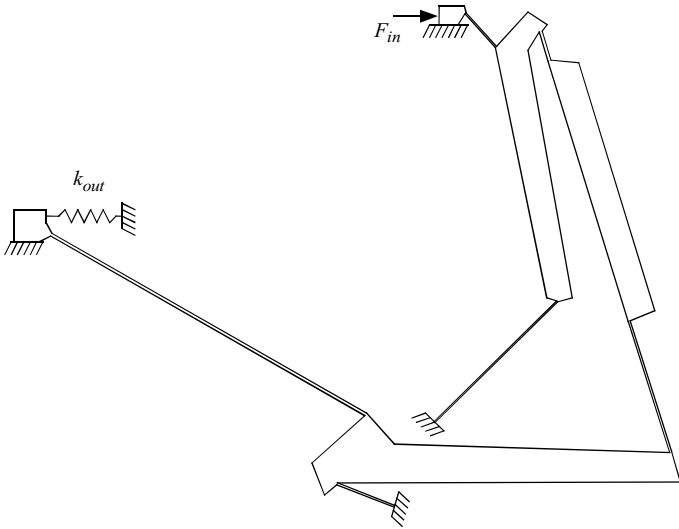


Figure 2. Optimal design for maximized force output using an output stiffness of 10 N/m.

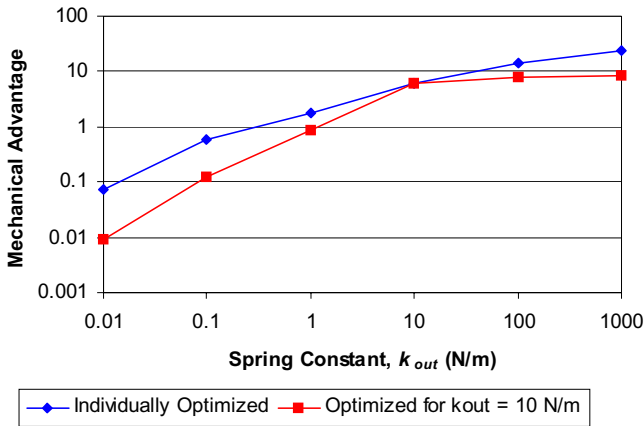


Figure 3. Uniqueness of optimal designs - mechanical advantage.

This design optimization was repeated using different values of the output spring constant k_{out} , with each solution of the optimization problem producing a unique design. The different values of k_{out} used for these optimization steps were $k_{out} = 0.01, 0.1, 1, 10, 100,$ and 1000 N/m. The resulting designs are indeed different from each other, as illustrated by Figure 3. The performance of the designs which were individually optimized for each value of k_{out} is plotted along with the performance of a single design (the design shown in Figure 2, optimized for $k_{out} = 10$ N/m) when it is attached to output springs of varying magnitude. The figure demonstrates that the single design does not span the space because its mechanical advantage when attached to different output springs is considerably less than the mechanical advantage of each

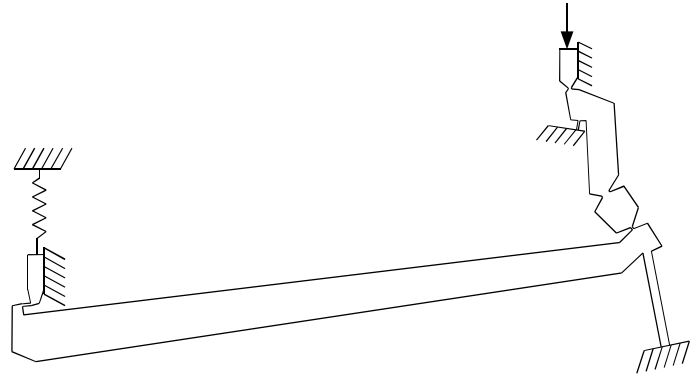


Figure 4. Optimal design for maximizing geometric advantage for an output stiffness of 10 N/m

individually optimized design. Therefore, a design tailored for the desired output load should be used to achieve the best performance. This is because the lengths and widths of the flexural pivots are optimized to support the given load. At lower loads, the pivots are too stiff, so that they require additional energy to deflect, while at higher loads they are not stiff enough, and do not adequately bear the output force.

Geometric Advantage

The procedure utilized to produce the optimal mechanical advantage designs for each of the design scenarios can be repeated to maximize geometric advantage. Eq. (1), with an objective function of GA instead of MA, is solved for each value of the parameter k_{out} . The resulting optimal design for $k_{out} = 10$ N/m is shown in Figure 4. This design has a geometric advantage of 30.27. As in the force example, each of the designs for different output loads is distinct to the spring constant utilized to obtain it. This is again illustrated by graphing the performance of the individually optimized designs against the single design, obtained when $k = 10$ N/m, operating under all k values (Figure 5).

Mechanical / Geometric Trade-off

The force amplification results detailed above are obtained at the expense of geometric advantage. For the case where $k = 10$ N/m and $F_{max} = 6.25$, the displacement is reduced by a factor of 0.114. Similarly, geometric advantage is obtained at the expense of mechanical advantage. For the same spring constant, the optimal geometric advantage is 30.27 and the corresponding force factor is 0.009342.

This trade-off can be explored for a given k_{out} by posing the optimization problem, Eq. (1), as a multicriteria optimization problem. The two objective functions are mechanical and geometric advantage. Each objective is weighted inversely proportional to the other and the sum of the two weights must always equal 1. When F_{max} has a weight of 1, G_{max} has a weight of 0 and the problem becomes a simple mechanical advantage maximization problem. The converse is also true. By varying

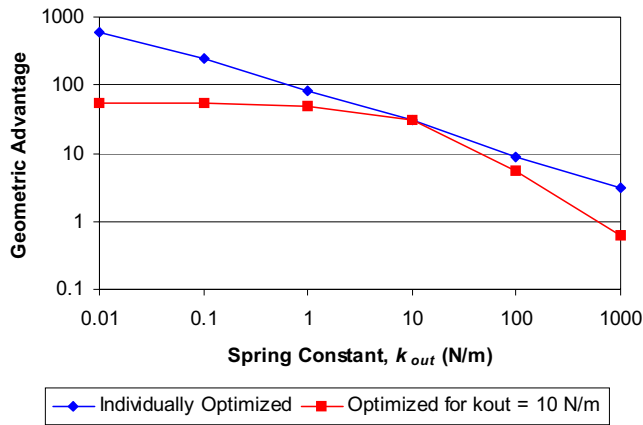


Figure 5. Uniqueness of optimal designs - geometric advantage.

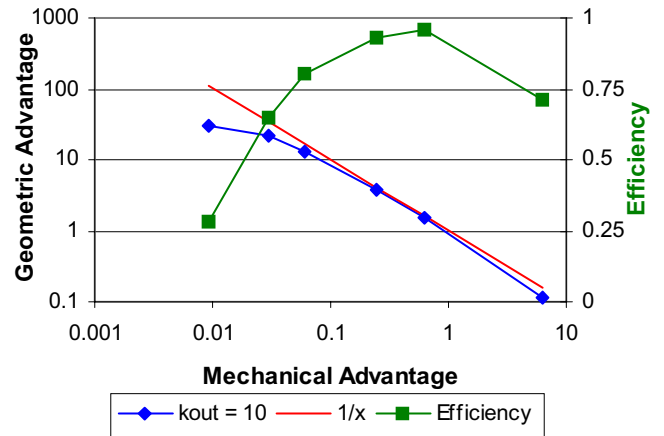


Figure 7. Log-log plot of Pareto set, $1/x$, and efficiency for $k = 10$ N/m.

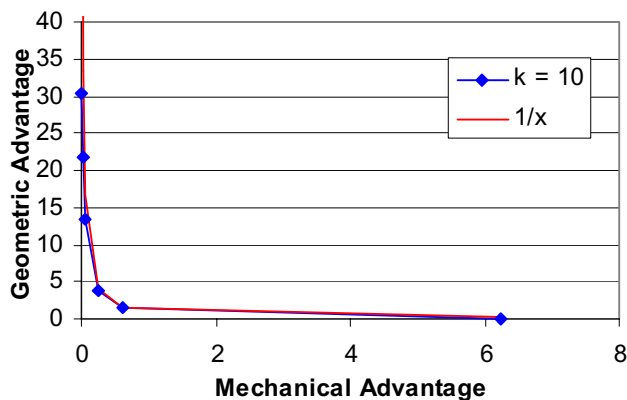


Figure 6. Pareto set of optimal designs graphed against best-possible performance, $1/x$.

these weights and solving the multicriteria problem, a Pareto set detailing the mechanical-geometric advantage trade-off is generated.

For a simple ideal lever, this trade-off has a $1/x$ relationship. The better the MEMS devices generated here perform, the more closely they will approach this ideal. A Pareto set for $k_{out} = 10$ N/m is shown in Figure 6, along with a graph of the line $1/x$. That the line representing the Pareto set, or family of optimal designs, is so close to $1/x$ indicates that the topology chosen for this device is efficient. The relationship in the two lines is more clearly seen in a log-log plot, Figure 7.

Another way of looking at the deviation of the Pareto-optimal designs from the ideal is through design efficiency. Efficiency is calculated by multiplying the mechanical and geometric advantages of a given design, and is a measure of how much of the input energy goes to the output. Efficiency for the $k_{out} = 10$ N/m design is plotted in Figure 7. The curves presented in Figure 7 and in the Appendix show that efficiency tends to be low for designs maximizing a single objective.

When both mechanical and geometric advantages are considered in the multicriteria objective function, efficiency improves. The efficiency for low k_{out} is much less than that for higher k_{out} designs. This may be due to the extremely weak output spring, which requires a much larger displacement to store the displacement to store the same amount of energy as compared to the other designs. Hence, a disproportionate amount of energy is used to deform the mechanism.

Pareto sets can be generated for each value of the parameter k_{out} (Figure 8). Taken together, these constitute a Pareto surface. Each point on this surface is an optimal design. Given a value for any two of the three axes (k_{out} , F_{max} , and G_{max}) the optimal value for the third can be read from the graph. Two dimensional plots of the Pareto set for each value of k_{out} are in the Appendix. They show how the nature of the designs change with the resistive load, k_{out} . As k_{out} increases, so does the mechanical advantage that the topology is able to achieve (to a maximum of 23.7). At the same time, the maximum geometric advantage decreases for these same designs. Likewise, as k_{out} decreases, geometric advantage increases (to a maximum of 588) and mechanical advantage decreases.

CONCLUSION

Size optimization of a prescribed compliant mechanism topology was performed in this paper to find designs which maximized geometric or mechanical advantage. The multicriteria optimization problem was also solved to develop the Pareto set for a wide range of output load stiffness. The results show that a single Pareto optimal design behaves very differently depending on the size of the output load. Thus, design optimization should be performed separately in different design problems to tailor the compliant mechanism to the input and output loads of each problem. The results presented here show the values of mechanical and geometric advantage which are possible for the given mechanism topology for many

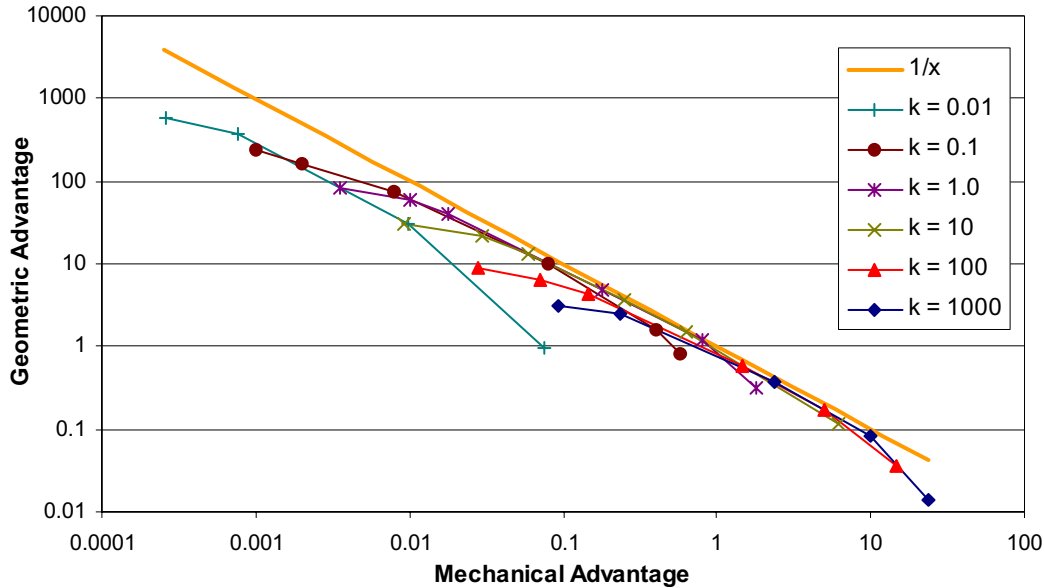


Figure 8. Mechanical / Geometric Advantage trade-off curves for each of the design scenarios considered.

different values of output stiffness. Each Pareto set showed behavior near the ideal $1/x$ curve, indicating that the prescribed topology performs well over a wide range of output loads.

The results also show that the geometric advantage of devices with low output stiffness tends to be much higher than that of designs with high output stiffness. Conversely, the mechanical advantage is larger for designs with stiff output resistance. This is because a stiff output spring develops force more quickly than a weak output spring, while a weak output spring deflects more easily than a stiff spring. This behavior is advantageous for design, where force amplification is generally desired in cases with a large output load, and displacement amplification is desired in case of a small output load which must be moved a long distance. Depending on the loading conditions, the topology investigated here allows geometric advantage as high as 588 and mechanical advantage as high as 23.7, allowing use in thermal or piezoelectric actuation, as well as force transducers such as accelerometers or tensile-test systems.

The efficiency of the Pareto-optimal designs, which relates input and output energy, was also studied. In general, the designs with weak output stiffness have a very low efficiency due to the large deflections required to store energy in the weak output springs. These large deflections require more of the input energy to be used to deflect the compliant mechanism. Also, each of the Pareto sets studied (at each value of k_{out}) showed a tapering of efficiency for designs which maximized mechanical or geometric advantage alone. Efficiency increased for multi-criteria optima, where both mechanical and geometric advantage were maximized subject to various weights. Hence, for a given design problem, either geometric or mechanical

advantage can generally be improved only at the expense of efficiency, creating a design trade-off in which the designer must choose the acceptable efficiency while still maximizing mechanism performance.

ACKNOWLEDGEMENTS

We would like to thank the Department of Mechanical Engineering at the University of Michigan for the use of computing resources used in this work. This work is supported under a National Science Foundation Graduate Research Fellowship.

REFERENCES

- [1] Roessig, T.A., Howe, R.T., Pisano, A.P., and Smith, J.H., 1997, "Surface-micromachined resonant accelerometer," *Intern. Conf. on Solid-State Sensors and Actuators*, 97TH8267, pp. 859-862.
- [2] Sato, K., Shikida, M., Yamasaki, M., and Yoshioka, T., 1996, "Micro tensile-test system fabricated on a single crystal silicon chip," *Proc. IEEE Micro Electro Mechanical Systems (MEMS) 1996*, 96CH35856, pp. 360-364.
- [3] Comtios, J.H., and Bright, V.M., 1997, "Applications for surface-micromachined polysilicon thermal actuators and arrays," *Sensors and Actuators, A: Physical*, vol. 58, no. 1, Jan. 1997, pp. 19-25.
- [4] Cragun, R., and Howell, L.L., 1999, "Linear Thermomechanical Microactuators," *Micro-electro-mechanical Systems*

(MEMS), 1999 ASME International Mechanical Engineering Congress and Exposition, pp. 181-188.

[5] Cragun, R., and Howell, L.L., 1998, "Constrained thermal expansion micro-actuator," *Micro-electro-mechanical Systems (MEMS)*, 1998 ASME International Mechanical Engineering Congress and Exposition, DSV vol. 66, pp. 365-371.

[6] Que, L., Park, J.-S., and Gianchandani, Y.B., 1999, "Bent-beam electro-thermal actuators for high force applications," *Proc. IEEE Micro Electro Mechanical Systems (MEMS) 1999*, 99CH36291, pp. 31-36.

[7] Chen, H. and Sun, P., 1996, "Design of two-layer flexible hinge milli-gripper," *Proc. Intern. Symp. Micro Machine and Human Science*, 96TH8213, pp. 99-104.

[8] Goldfarb, M. and Lipsey, J.H., 1997, "Design of a minimum surface-effect tendon-based microactuator for micromanipulation," *Proc. IEEE Intern. Conf. on Robotics and Automation*, 97CH35992, pp. 1460-1465.

[9] King, T., Pozzi, M., and Manara, Angelo, 2000, "Piezoactuators for real-world applications: Can they deliver sufficient displacement?," *Power Engineering Journal*, vol. 14, no. 3, pp. 105-110.

[10] Capelleri, D.J., Frecker, M.I., and Simpson, T.W., 2000, "Optimal design of a PZT bimorph actuator for minimally invasive surgery," *Proc. SPIE - Smart Structures and Materials 2000 - Mathematics and Control in Smart Structures*, vol. 3984, pp. 321-335.

[11] Huang, X.T., Saif, M.T., and MacDonald, N.C., 1996, "Micromotion amplifier," *Proc. IEEE Micro Electro Mechanical Systems (MEMS)*, 96CH35856, pp. 424-428.

[12] Kota, S., Hetrick, J., Li, Z., Rodgers, S., and Krygowski, T., 2000, "Synthesizing high-performance compliant stroke amplification systems for MEMS," *Proc. IEEE Micro Electro Mechanical Systems (MEMS) 2000*, 00CB36308, pp. 164-169.

[13] Ananthasuresh, G.K. and Kota, S., 1996, "The Role of Compliance in the Design of MEMS," *Proceedings of the 1996 ASME Design Engineering Technical Conferences*, 96-DETC/MECH-1309.

[14] Kota, S., Hetrick, J., Li, Z., and Saggere, L., 1999, "Tailoring unconventional actuators using compliant transmissions: design methods and applications," *IEEE/ASME Transactions on Mechatronics*, vol. 4 no. 4, pp. 396-408.

[15] Canfield, S. and Frecker, M., 2000, "Topology optimization of compliant mechanical amplifiers for piezoelectric actuators," *Structural and Multidisciplinary Optimization*, vol. 20, no. 4, pp. 269-279.

[16] Howell, L.L. and Midha, A., 1994, "A Method for the Design of Compliant Mechanisms with Small-Length Flexural Pivots," *ASME Journal of Mechanical Design*, Vol. 116, No. 1, pp. 280-290.

[17] Sharpe, W.N. Jr., Brown, S., Johnson, G.C., and Knauss, W., 1998, "Round-robin tests of modulus and strength of polysilicon," *Microelectromechanical Structures for Material Research*, MRS vol. 518, pp. 57-65.

[18] Kirkpatrick, S., Gelatt, C.D., and Vecchi, M.P., 1983, "Optimization by Simulated Annealing," *Science*, vol. 22, no. 459, p. 671.

[19] Parkinson, A.R., and Wilson, M., 1988, "Development of Hybrid GRG-SQP Algorithm for Constrained Nonlinear Programming," *J of Mech. Trans. and Automation in Design*, Trans. ASME, vol. 110, p. 308.

APPENDIX

